Comparative Analysis of Genetic Variations in the $Na_v1.5$ Sodium Channel Subunits that Underlie Brugada Syndrome Using Patient-Specific iPSC-CMs

Yue Zhu
Jiangsu Province Hospital and Nanjing Medical University First Affiliated Hospital
Linlin Wang
Nanjing Medical University Affiliated Brain Hospital, Nanjing Chest Hospital
Chang Cui
Jiangsu Province Hospital and Nanjing Medical University First Affiliated Hospital
Shaojie Chen
Jiangsu Province Hospital and Nanjing Medical University First Affiliated Hospital
Hongwu Chen
Jiangsu Province Hospital and Nanjing Medical University First Affiliated Hospital
Huiyuan Qin
Jiangsu Province Hospital and Nanjing Medical University First Affiliated Hospital
Yongping Lin
Jiangsu Province Hospital and Nanjing Medical University First Affiliated Hospital
Hongyi Cheng
Jiangsu Province Hospital and Nanjing Medical University First Affiliated Hospital
Xiaohong Jiang
Jiangsu Province Hospital and Nanjing Medical University First Affiliated Hospital
Minglong Chen (chenminglong@njmu.edu.cn)
Jiangsu Province Hospital and Nanjing Medical University First Affiliated Hospital

Research

Keywords: Brugada Syndrome, quinidine, SCN5A, SCN1B, iPS

Posted Date: September 3rd, 2020

DOI: https://doi.org/10.21203/rs.3.rs-70177/v1

Abstract

Background: Brugada syndrome (BrS) is an autosomal dominant disorder that causes a high predisposition to sudden cardiac death. Several genes have been reported to be associated with BrS. Considering that the heterogeneity in clinical manifestations may result from genetic variations, the application of patient-specific induced pluripotent stem (iPS) cell-derived cardiomyocytes (CMs) may help to reveal cell phenotype characteristics resulting from different genetic backgrounds. The present study was to compare the structural and electrophysiological characteristics of sodium channel subunits with different genetic variations and evaluate the safety of quinidine for use with BrS patient-specific iPSC-derived cardiomyocytes.

Methods: Two BrS patient-specific iPS cell lines were constructed that carried missense mutations in *SCN5A* and *SCN1B*. One iPS cell line from a healthy volunteer was used as a control. The differentiated cardiomyocytes from the three groups were evaluated by flow cytometry, immunofluorescence staining, electron microscopy, as well as calcium transient and patch clamp analyses to assess different pathological phenotypes. Finally, we evaluated the drug responses to varying concentrations of quinidine by measuring the action potential.

Results: Compared to the control group, BrS-CMs showed a significant reduction in sodium current, prolonged action potential duration and varying degrees of decreased Vmax, but no structural difference was observed. After applying different concentrations of quinidine, the disease-specific groups and the control group had a downward trend in maximal upstroke velocity, resting membrane potential and action potential amplitude, and exhibited prolonged action potential duration without increasing incidence of arrhythmic events.

Conclusion: Both patient-specific iPSC-CMs recapitulated the BrS phenotype at the cellular level. Although the *SCN5A* variation led to a markedly lower sodium current than what was observed with the *SCN1B* variation, their responses to quinidine were quite similar. The present study provides an advantageous platform for exploring disease mechanisms and evaluating drug safety *in vitro*.

Introduction

Brugada syndrome (BrS) is an inheritable cardiac condition characterized by a typical electrocardiogram of right bundle branch block (RBBB) with ST-segment elevation in V1-V3(1). BrS is associated with a high incidence of polymorphic ventricular tachycardia (VT) or ventricular fibrillation (VF), which leads to sudden cardiac death, especially in young men(2). The implantation of a cardiac defibrillator (ICD) is the only established treatment(3). However, shock from ICD is painful and may cause post-ICD shock stress reactions(4). Alternatively, drugs that counteract the ionic current imbalance may be efficient. Currently, quinidine is applied in BrS patients to prevent the electrical storm of ICD, but its effectiveness and safety are controversial(5).

Genetic studies have revealed that BrS is associated with variations in multiple genes, including *SCN5A*, *SCN1B*, *CACNA1C*, and *KCND3*(6). The most commonly involved gene in BrS is *SCN5A*, which encodes the α-subunit of the voltage-gated cardiac sodium channel ($Na_v1.5$) (7). Recently, we reported that a single nucleotide variant (A197V) in *SCN1B*, encoding the β1-subunit of $Na_v1.5$, is responsible for BrS susceptibility(8). Such loss of function of the sodium channel would result in impaired depolarization and a prominent transient-outward current (Ito), which was found to be the basis of a possible phase two reentry that triggers VT episodes(9). However, the characterization of cardiomyocytes with genetic variations in different subunits of $Na_v1.5$ remains to be compared.

While conventional heterologous expression provided insights into single-channel function, it fails to reflect the changes in whole membrane potential and electrical-mechanical coupling. Thus, human cardiomyocytes, especially patient-specific cardiomyocytes, are needed to explore the mechanisms underlying the ion channel diseases. Indeed, the emergence of human induced pluripotent stem cells (iPSCs) provides a promising tool for recapitulating the phenotype of cardiac disease and for evaluating the efficiency of drug treatments (10–12). In recent years, BrS patient-specific iPSC-CMs have been reported to be accurate disease models *in vitro* (13, 14). However, their drug responses to quinidine have not been fully elucidated.

In the present study, we recruited two Brugada patients who carry missense mutations in *SCN5A* and *SCN1B*. We generated patient-specific iPS cell lines and differentiated them into ventricular cardiomyocytes. Through structural and electrophysiological assessments, we investigated the pathological properties of BrS at the cellular level. By evaluating the drug responses to quinidine *in vitro*, we highlighted the efficacy and safety of quinidine treatment in BrS-CMs.

Methods

Generation of human iPS cell lines

The human iPS cell lines used in this study were derived from the peripheral blood mononuclear cells of two Brugada patients and one healthy volunteer. The approval of the study was provided by the Bioethics Committee of the First Affiliated Hospital of Nanjing Medical University (2014-SR-090). The iPSC lines were generated using a CytoTune™-iPS 2.0 Sendai Reprogramming Kit (Thermo Fisher Scientific, A16517), which employed four Yamanaka factors (OCT4, KLF4, SOX2 and cMYC), following the manufacturer's instructions with subtle adjustments. Reprogrammed PBMCs were replated onto Matrigel (Corning, Corning, NY, USA, 354277) coating plates, and the medium was changed to mTeSR™1 (STEMCELL Technologies Inc., Vancouver, Canada, 05850) after transduction. Individual colonies could be identified on day 7 and were picked 20 days later and were maintained in mTeSR™1 medium.

Genome sequencing

To confirm the presence of the variations in the two iPS cell lines, patient-derived iPSCs were examined by Sanger sequencing. Total DNA was isolated using a TIANamp Genomic DNA Kit (TIANGEN Biotech, BJ,

China), and the coding regions of SCN5A and SCN1B, including each variation site, were amplified by polymerase chain reaction (PCR). The PCR products were purified using a DNA Purification Kit (TIANGEN Biotech) and then were sequenced. The results were compared with the SCN5A and SCN1B reference sequences NM_001099404 and NM_001037.

Differentiation of hiPSC-CMs

A monolayer-based cardiomyocyte differentiation protocol was applied as previously described. Briefly, iPSCs were allowed to grow to over 90% confluence in mTeSR™1 medium and then were switched to RPMI 1640 medium (Gibco, 1744361) containing B-27® supplement without insulin (Gibco, A1895601). On day 0–1, additional CHIR-99021 (6 μM, Selleckchem, S2924) was added to induce mesodermal differentiation. On days 3–4, IWR-1 (5 μM, Sigma-Aldrich, 10161) was added to the medium to inhibit Wnt signaling and induce cardiogenesis. From day 8 onward, cells were cultured in RPMI 1640 containing B27® complete supplement (Gibco, 17504-044), and the medium was refreshed every other day. Beating cardiomyocytes could be observed from approximately days 8 to 10. Cells were cultured for at least 8 weeks and were dissociated using 0.25% trypsin-EDTA for further functional and electrophysiological analyses.

Flow cytometry analysis

Cells were treated with the appropriate dissociation solution (Accutase for iPS cells, 2.5% trypsin for CMs) and fixed with 4% paraformaldehyde at room temperature for 20 min. Pluripotent stem cells were counted and stained using antibodies against SSEA-4 (1:50 dilution, phycoerythrin conjugated, Miltenyi Biotec, FAB1435P-025) for 30 min at 4°C shielded from light. Cardiomyocytes were co-incubated with anti-cTnT-FITC (1:50, Miltenyi Biotec, 130-106-687) and anti-MLC2v-PE (1:50, Miltenyi Biotec, 130-106-133) in PBS at 4 °C for 30 min. REA Control-FITC (1:50, Miltenyi Biotec, 130-104-611) and REA Control-PE (1:50, Miltenyi Biotec, 130-104-613) were used as isotype controls. The cells were measured using FACSCalibur (BD, Franklin Lakes, NJ, USA) and subsequent analysis were performed using FlowJo software(Tree Star, version 10.5.3).

Immunofluorescence staining

Cells were seeded on a coverslips and cultured for 3–5 days before being fixed in 4% paraformaldehyde for 20 min. The cells were permeabilized with 0.1% Triton X-100 for 5 min, when needed. Cells were then blocked in 5% BSA in PBS for 30 min; all of these steps occurred at room temperature. Cells were then incubated overnight at 4 °C with primary antibodies. For pluripotent stem cells, anti-SSEA4 (1:200, Abcam, ab16287), anti-Oct4 (1:200, Abcam, ab200834), anti-Nanog (1:200, Abcam, ab109250) and TRA-1-81 monoclonal antibody (1:150, Thermo Fisher Scientific, MA1-024) were applied. For cardiomyocytes, anti-α-actinin (1:200, Sigma-Aldrich, A7811), anti-cardiac troponin T (1:200, Abcam, ab8295), anti-MLC2v (1:200, Abcam, ab79935) were used. The following secondary antibodies include Alexa Fluor® 488 goat anti-rabbit IgG (1:800, Abcam, ab150077) and Alexa Fluor® 555 goat anti-mouse IgG (1:800, Abcam, ab150118) were incubated with samples at room temperature for 30 min. The nuclei were stained with DAPI (Life Technologies, P36931). Then, the cells were rinsed with PBS and observed under a

fluorescence microscope (Axio Imager A2, Carl Zeiss, Germany). Images were analyzed and merged with ImageJ (NIH, version 1.8.0_77).

Transmission electron microscopy (TEM)

Cardiomyocytes were prepared for TEM evaluation as described previously(15). Briefly, CMs were dissociated into single cells with 0.25% trypsin. Samples were then fixed with 2.5% glutaraldehyde (Sigma-Aldrich), post fixed with 1% osmium tetroxide and rinsed with PBS. After dehydration with a series of ethanol solutions and embedding into resin, ultrathin sections were cut with an ultramicrotome (Leica EM UC7; Leica, Wetzlar, Germany) and stained with lead citrate. Visualization was performed under a transmission electron microscope (JEM-1010, Jeol Ltd., Tokyo, Japan) equipped with a CCD camera operated at 75 kV.

Patch clamp analysis

Three to four days after dissociation, single cell patch clamp experiments were performed using an Axopatch 200B amplifier (Axon Instruments, Union City, CA, USA) and analyzed with Clampfit 10.3 software (Molecular Devices, Sunnyvale, CA). Glass pipettes were pulled using borosilicate glass (Sutter Instrument Co, Novato, CA) and a micropipette puller (Model P-100, Sutter Instruments, Novato, CA, USA). Pipettes with resistance ranging from 2–4 MΩ were perfused with specified intracellular solutions and were used.

Na measurement

The sodium currents (I_{Na}) of cardiomyocytes were recorded using a whole-cell patch-clamp technique at room temperature as previously described(8). Data were filtered at 2 kHz and acquired at 20 kHz. I_{Na} was examined using the following intracellular solution designed to eliminate the outward potassium current: 60 mM CsCl, 60 mM CsF, 10 mM TEA-Cl, 1 mM $CaCl_2$, 1 mM $MgCl_2$, 10 mM EGTA, 10 mM glucose, and 10 mM HEPES (pH 7.2 with CsOH). The external bath solution composition was as follows: 130 mM choline chloride, 10 mM NaCl, 1 mM TEA-Cl, 1.8 mM $MgCl_2$, 1.8 mM $CaCl_2$, 0.2 mM NiCl, 10 mM glucose, and 10 mM HEPES (pH 7.2 with NaOH). Nifedipine was added to exclude inward calcium current. The program for recording I_{Na} ranged from − 80 to + 40 mV in 10 mV increments that occurred every 50 ms. Cell capacitance was measured to normalize I_{na} by applying a 10 mV voltage step from − 100 mV, and current density was calculated as peak current divided by cell capacitance (pA/pF).

AP measurement

Spontaneous action potentials were recorded at 37 °C in Tyrode's solution as previously described (16). Data were filtered at 5 kHz and digitized at 40 kHz. Pipettes were filled with the following internal solution (in mM): 150 KCl, 5 NaCl, 2 $CaCl_2$, 5 MgATP, 5 HEPES, 5 EGTA, and 10 glucose (pH 7.2 with KOH). APs were characterized by resting membrane potential (RMP), maximum AP amplitude (APA), maximum upstroke velocity (V_{max}) and average action potential duration at 90%, 50%, and 30% repolarization (APD90, APD50, APD30, respectively). Each average data was from 10 consecutive recorded APs.

Calcium transient

Cells were loaded with the calcium-sensitive dye fluo-4 AM (Life Technologies, F14201) at a working concentration of 5 μM for 60 min at 37 °C. After rinsing the iPSC-CMs, they were maintained in Tyrode's solution. The spontaneous calcium fluorescence signal was recorded by an inverted fluorescence microscope (Axio Vert. A1, Carl Zeiss, Jena, Germany) equipped with an sCMOS camera (Tucsen, Dhyana95, China). The excitation and emission wavelengths of Fluo-4 were 488 nm and 505 nm, respectively. Recordings were obtained at the acquisition rate of 25 frames/second for a 15 second duration. To calibrate the cell-to-cell variability and background disturbance, the fluorescence intensity in the region of interest was determined based on the formula: (F-F0)/F0. Herein, F0 represents the baseline intensity, while F represents the intensity at any point in time. The parameters that describe and evaluate the calcium transient include the spontaneous beat rate, amplitude and arrhythmic events that are EAD-like or fibrillation-like. Data were analyzed using ImageJ as previously described(15).

Drug response

Quinidine (Selleckchem, S4658) was dissolved in dimethyl sulfoxide (DMSO) to prepare a 100 mM stock solution. Working solutions were freshly prepared in cell-specific medium. Final concentration was set as 0.1-fold to 10-fold the ETPC (unbound effective therapeutic plasma concentration) of quinidine (0.3, 1, 3,10, 30 μM). Dilutions ratio up to 1000 had no effect on cell apoptosis or cardiac electrical activity.

Baseline AP was recorded for each cell before the treatment. Then, quinidine was sequentially applied from the lowest to highest concentration at 10-min intervals for washout to obtain a steady state. For each concentration, 10 recorded APs from each cell were averaged for analysis. The following parameters were quantitated as mentioned above: RMP, APA, $V_{max,}$ APD30, APD50 and APD90. Recordings at each concentration were normalized to their baseline.

Statistical Analysis

Data with a normal distribution were presented as the mean ± SEM. One-way ANOVA was used to compare parameters among the test groups (i.e. the control, SCN1B, and SCN5A groups). Chi-square test was used for categorical variables. For pharmaceutical experiments, the post-drug effects were evaluated by comparing to the baseline using a paired Student's t test. All statistical analyses were performed with R (version 4.0.2) and significance was determined at a $P < 0.05$.

Results

Clinical and genetic profiles

Two BrS patients and one healthy volunteer were recruited to the present study. The diagnosis of Brugada syndrome was made based on the 2005 consensus diagnostic criteria(17). Patient 1 (BrS1) was a 42-year-old man presenting with unstable VT after multiple episodes of recurrent syncope. His resting ECG showed a characteristic type 1 Brugada pattern (Fig. 1a, left panel). Moreover, pedigree investigation

showed that his brother died from sudden cardiac death. Patient 2 (BrS2) was a 46-year-old man with a history of recurrent syncope. The resting ECG exhibited a typical type 1 Brugada ECG pattern (Fig. 1a, right panel). Both patients received ICD implantation and close follow-up. Genetic testing revealed a *SCN5A* V1405M (c.4213G > A) variation in BrS1 and a *SCN1B* A197V (c.590C > T) variation in BrS2. The corresponding positions of each variation on the protein structure of the Nav1.5 sodium channel α subunit or β-1 subunit are illuminated in Fig. 1c.

Our healthy control subject was a young woman with normal ECGs and without personal or family history of sudden death. Whole-genome sequencing indicated no disease-causing variants in any cardiovascular-related genes.

Characterization of iPS cell lines

Human iPSCs were generated from PBMCs derived from the two patients and the healthy controls. The iPSC lines showed a normal karyotype and stem cell morphology (Fig. 2a). To verify the pluripotency of each iPS cell line, undifferentiated stem cells were fixed and stained. As expected, cells from both the BrS and control groups expressed the robust pluripotency markers NANOG, OCT-4, SSEA4 and TRA-1-81 (Fig. 2b and Figure S1). Further flow cytometry analysis revealed a high proportion (> 95%) of SSEA-4-positive cells in each group (Fig. 2c). Genetic testing confirmed the variation sites of *SCN5A* c.4213G > A and *SCN1B* c.590C > T in the corresponding iPSC lines, indicating that reprogramming maintained the genetic variations found in the BrS patients (Fig. 1b).

Structural analysis of BrS-CMs

Highly efficient cardiac differentiation was conducted. FACS analysis of the cardiac-specific marker cTnI and ventricular cardiomyocyte marker MLC2v confirmed the purity of ventricular myocytes to be over 90% (Fig. 3a). Considering the immaturity of newly differentiated cardiomyocytes, prolonged cultivation up to 60 days was applied. To compare the morphological properties of the cells, we stained age-matched cells for cardiac structural proteins α-actinin, cTnI and MLC2v. All cells exhibited robust expression of these markers with organized striation patterns of sarcomeres (Fig. 3b).

Furthermore, we examined the cardiac ultrastructures using transmission electron microscopy. In both BrS and control iPSC-CMs, myofibrils were well organized with aligned linear Z-discs (Fig. 3c). Abundant mitochondria and sarcoplasmic reticulum could be seen around the sarcomere. Given the above findings, we report no significant discrepancy in morphology between control and both BrS cardiomyocytes.

BrS-CMs showed impaired Na^+ current

To compare the impact of different variations in the $Na_v1.5$ subunits on sodium current, we measured the sodium current using voltage clamp experiments. Figure 4a plots representative I_{Na} traces for BrS and control cardiomyocytes at varying potentials. It demonstrated a loss of function of the sodium channel current in both the SCN1B and SCN5A groups compared to control-derived cardiomyocytes (Fig. 4b). Further analysis demonstrated that peak I_{Na} density was reduced by 80% in BrS-SCN5A and 70% in BrS-

SCN1B compared to their control counterparts (Fig. 4c). Notably, the peak I_{Na} density of BrS-SCN5A cardiomyocytes was even lower than that of the SCN1B group. In addition, we assessed the transient outward current (Ito), which is judged as another potentially contributing factor of BrS. The results demonstrated that Ito currents were not significantly changed in either BrS cell line compared with the control (Figure S2).

BrS-CMs exhibited abnormal action potential

To investigate whether $Na_v1.5$ variations would affect the whole membrane potential, we next recorded action potentials by patch clamp (Fig. 5a). Only ventricular-like cardiomyocytes were studied. In line with our sodium current data, APA (Fig. 5b) and Vmax (Fig. 5c) were significantly decreased in the BrS groups compared to the control group. Action potential durations (APD 30, 50 and 90) were significantly longer in both BrS cell groups than they were in the healthy control (Fig. 5d). Besides, comparing to the control group, both BrS groups displayed a high incidence of arrhythmic events including early afterdepolarizations (EADs) or delayed afterdepolarizations (DADs)(0 out of 10 for control, 3 out of 10 for BrS-SCN5A, 2 out of 9 for BrS-SCN1B)(Fig. 7g ~ 7i). To sum up, these results indicated that BrS iPSC-CMs exhibited notably aberrant AP phenotypes. Meanwhile, the action potentials from the BrS-SCN1B and BrS-SCN5A groups presented the same pattern. All the AP characterizations are summarized in Table S1.

BrS-CMs exhibit altered Ca^{2+} handling

Considering that calcium is a critical mediator of excitation-contraction coupling in cardiac cells, we then examined the changes in intracellular calcium concentration using calcium probes. The representative curves of Ca^{2+} handling from each group are shown in Fig. 6a. Both BrS iPSC-CMs exhibited similar peak amplitudes compared to those of control cells (Fig. 6b). Nevertheless, the kinetic stability of calcium handling was disturbed in the BrS groups. As shown in Fig. 6a, BrS cells exhibited more proarrhythmic events, including delayed afterdepolarization-like and early afterdepolarization-like events, than controlled CMs. The percentages of cells showing proarrhythmic events in BrS-SCN5A, BrS-SCN1B and control cells were 58%, 46%, and 3%, respectively, $p<0.05$ for chi-square test (Fig. 6c).

Cardiac safety evaluation of quinidine using BrS-CMs

Quinidine is a class 1A antiarrhythmic drug with significant Ito blocking properties, and it is reported to be effective for preventing life-threatening ventricular arrhythmias due to Brugada syndrome. As a result, oral quinidine therapy was applied to both BrS1 and BrS2 patients after their ICD implantation. During follow-up, there was no report of ICD discharge in these two patients. Meanwhile, quinidine also blocks potassium channels in phase 3. Recent studies reported that quinidine-induced QT prolongation increased the risk of fatal arrhythmia(18). Hence, further investigation of drug safety is warranted before the prescription of lifetime drug use.

Human iPSC-CMs are considered to be precise tools for cardiac safety drug screening *in vitro*. To further confirm the drug safety of quinidine for treatment of cells with these two variations, hiPSC cardiomyocytes were subjected to varying concentrations of quinidine, ranging from 0.3 to 30 μM. The

results demonstrated that quinidine had no impact on cell viability when examined by CardioExcyte 96 (Figure S3). Action potential was further analyzed to detect drug effects on cellular electrophysiology. As shown in Fig. 7a ~ 7f and Table S2, quinidine decreased the V_{max}, APA and RPM in a concentration-dependent manner among the three groups. Interestingly, APD90 was prolonged in all cell lines with increase of quinidine concentration, and then showed a downward trend when the concentration reached 3-fold the ETPC (10 μM) or higher. Besides, the control group had a greater prolongation of APD90 when comparing with both BrS groups(P 0.05). All the groups showed similar mild changes in both APD30 and APD50. In addition, both BrS-CMs treated with quinidine within 3-fold the ETPC eliminate spontaneously occurring triggered events(Fig. 7g ~ 7i). These results highlighted that quinidine had positive effects in BrS-CMs with insurance of safety.

Discussion

BrS is an inherited ion channelopathy associated with a propensity for developing fetal ventricular arrythmias. Herein, we performed the first comparison of the cell physiology and pharmacological properties of iPSC-CMs derived from two BrS patients carrying different variations in sodium channel-associated genes. Our results demonstrated that iPSC-CMs derived from different genotypes of BrS patients recapitulated the human disease phenotype, including the prolongation of APD, impairment of I_{Na}, and high prevalence of proarrhythmic events. Additionally, our study provided a comprehensive evaluation of quinidine on BrS-CMs, supporting the safety of the drug for lifelong use.

Relatively mature phenotype by prolonged cultivation of iPSC-CMs

It is well known that newly differentiated iPSC-CMs are more fetal-like in phenotype than adult cardiomyocytes, which has impeded the widespread use of hiPSC-CMs for scientific studies(19, 20). Currently, prolonged culturing is the most accessible and easy approach for prompting cardiac maturation(21). In the present study, the cells were cultivated until 60 days with *in vitro* differentiation to obtain a relatively mature state. Our morphological analysis indicated that the structures of BrS-CMs were normal. On the other hand, the organized sarcomeres together with ultra-micro aligned Z-disc structures indicated that the D60 cardiomyocytes exhibited a high degree of maturity. We have reported that ion channel function relies on the iPSC-CM maturation status(22). Thus, applying such relatively mature CMs for disease modeling would be highly reliable.

Electrophysiological abnormalities caused by $Na_v1.5$ gene variations

In the electrophysiological assessment part of the study, we found that the changes in the sodium channels of BrS patients were consistent with the findings of previous studies (all from *SCN5A*-mutant iPSCs) (23). It is worth mentioning that iPSC-CM carrying the *SCN1B* missense mutation also had a significant decrease in sodium current, although the decline was not as obvious as that of *SCN5A* mutant

BrS-CMs. This could be explained by the fact that *SCN1B* encodes only the accessory subunit of the sodium channel(24).

Compared to the use of I_{Na} as a single parameter, action potential can reflect the impact of variants on the entire cellular electrophysiology, including the compensation of other ion channels to the sodium current impairment. Our study illuminated the abnormality in AP profiles of BrS-CMs, which is in line with previous studies(25). The BrS-CMs also presented a prolonged AP duration, which seems to be an overlapping feature of long QT type 3 and BrS(26) (27). Moreover, BrS-CMs exhibited multiple abnormal calcium-related activities, including EAD-like and DAD-like events, which are thought to be a surrogate for polymorphic VT(28, 29). Collectively, both $Na_v1.5$ gene mutants in our study impaired electrophysiological function and triggered adverse events related to BrS clinical manifestations.

Pharmacologic responses to quinidine

The pharmacologic basis of treating BrS is aimed at justifying outward and inward currents of the epicardium by reducing the outward Ito current or increasing the inward I_{Ca} current(30). Quinidine, a class IA antiarrhythmic agent with significant Ito blocking properties, is reported to reduce electrical heterogeneity, restore synchrony and terminate phase 2 reentrant activity(31). However, the use of quinidine could induce prolongation of the QT interval, which can result in the initiation of ventricular arrhythmia(32, 33). Since BrS is a genetic condition, the discrepancy in drug response may result from the different genetic backgrounds. In our study, we performed quinidine testing in BrS-CMs with different sodium channel gene variations and compared them to cells from healthy donors. We found that all the cell lines showed depressed phase 0 depolarization after quinidine treatment. APD90 presented with a concentration-dependent prolongation caused by quinidine, which is the result of inhibition of sodium channel in phase 0 and potassium channel in phase 1 and 3. It is worth mentioning that the prolongation was more profound in the control cells. The downward trend appeared when the concentration reached 10 μM, we infer that the L-type calcium channel was blocked by quinidine at such concentration according to previous descriptions(34). There was no prominent effect on APD30 or APD50. These findings were in line with the drug experiment in human ventricular trabeculae(35), indicating the pronounced blockade of potassium current especially hERG than the sodium current. Besides, we observed that adverse events were reduced or at least not added in the range of 3-fold the ETPC of quinidine in BrS-CMs, and were even newly emerged in control group. These findings support the idea that quinidine is an effective and safe drug for BrS patients.

Study limitations

First, genotype might not equal pathogenesis. A low prevalence of mutation carriers leads to an ambiguous relationship between genotype and phenotype. Patients in the absence of any mutation may have an anatomic structural variant in the RV outflow track that is sufficient for pathogenesis(36). However, we believe that the genetic basis was an important contributor to the pathogenesis of BrS. It is reported that the heterogeneity expression in Nav1.5 expression could determine the conduction heterogeneities in different regions(37). Second, our present model can enable study at a cellular level but

not an organ or tissue level. Previous studies performed in a canine ventricular wedge model successfully captured the BrS ECG pattern(38). However, it is unable for a monolayer of iPSC-CMs to achieve such signals *in vitro*. Hopefully, the pathophysiological changes recapitulated here can be coupled with new techniques for engineering heart tissue.

Conclusion

In summary, our study compared the phenotype of hiPSC-CMs carrying variations of *SCN5A* and *SCN1B*. Both patient-specific iPSC-CMs recapitulated the BrS phenotype on a cellular level, including impaired I_{Na}, abnormal action potential parameters, increased arrhythmia events, and effective responses to quinidine. Our findings help to understand the mechanisms of BrS at the cellular level and support patient-specific iPSC-CMs as a promising platform for drug testing and therapeutic target exploration.

Abbreviations

Brugada syndrome: BrS; RBBB: right bundle branch block; VT: ventricular tachycardia; VF: ventricular fibrillation; ICD: Implantable cardioverter defibrillator; ECG: electrocardiogram; $Na_v1.5$: voltage-gated cardiac sodium channel; I_{Na}: sodium current; Ito: transient outward potassium current; I_{Ca}: calcium current; AP: Action potential; APA: Action potential amplitude; APD: Action potential duration; RPM: resting membrane potential; V_{max}: maximum upstroke velocity; iPSC: Induced pluripotent stem cell; CM: cardiomyocyte; RV: Right ventricular; TEM: Transmission electron microscopy; ETPC: unbound effective therapeutic plasma concentration; EADs: early afterdepolarizations; DADs: delayed afterdepolarizations.

Declarations

Acknowledgements

Authors would like to thank Dr. Qun Lu for providing scientific feedback.

Funding

The work was supported by Natural Science Foundation of Jiangsu Province of China (grant number BK20160134 to LW and BK20191071 to CC, http://www.jstd.gov.cn/), National Natural and Science Foundation of China (grant number 81900295 to CC, http://www.nsfc.gov.cn/), and Special Foundation for Clinical Science and Technology of Jiangsu Province (grant number, BE2017754 to HC, http://kxjst.jiangsu.gov.cn/).

Availability of data and materials

All data generated or analyzed in this study are included in this published article and its supplementary information files, which are available from the corresponding author upon reasonable request.

Authors' contributions

YZ generated the hiPSC lines, performed the experiments, analyzed the data and prepared the manuscript. LW and HQ performed the patch-clamping experiments. CC analyzed the data and contributed to the writing. YL, HC and XJ differentiated the iPSC-derived cardiomyocytes. HC contributed to the writing of the manuscript. MC supervised the work and wrote the manuscript. All authors read and approved the final manuscript.

Competing interests

The authors declare that they have no competing interests.

Consent for publication

Not applicable.

Ethics approval and consent to participate

All research involving human stem cells complied with the International Society for Stem Cell Research "Guidelines for the Conduct of Human Embryonic Stem Cell Research". Human iPSC lines used in this study are derived from peripheral blood mononuclear cells of healthy humans with written consent previously approved by the Bioethics Committee of the First Affiliated Hospital of Nanjing Medical University (2014-SR-090).

References

1. Brugada P, Brugada J. Right bundle branch block, persistent ST segment elevation and sudden cardiac death: a distinct clinical and electrocardiographic syndrome. A multicenter report. J Am Coll Cardiol. 1992;20(6):1391-6.
2. Antzelevitch C. Brugada syndrome. Pacing Clin Electrophysiol. 2006;29(10):1130-59.
3. Brugada J, Brugada R, Brugada P. Pharmacological and device approach to therapy of inherited cardiac diseases associated with cardiac arrhythmias and sudden death. J Electrocardiol. 2000;33 Suppl:41-7.
4. Olde Nordkamp LR, Postema PG, Knops RE, van Dijk N, Limpens J, Wilde AA, et al. Implantable cardioverter-defibrillator harm in young patients with inherited arrhythmia syndromes: A systematic review and meta-analysis of inappropriate shocks and complications. Heart Rhythm. 2016;13(2):443-54.
5. Sieira J, Brugada P. Management of Brugada Syndrome 2016: Should All High Risk Patients Receive an ICD? All High-Risk Patients Should Receive an Implantable Cardiac Defibrillator. Circ Arrhythm Electrophysiol. 2016;9(11).
6. Gourraud JB, Barc J, Thollet A, Le Scouarnec S, Le Marec H, Schott JJ, et al. The Brugada Syndrome: A Rare Arrhythmia Disorder with Complex Inheritance. Front Cardiovasc Med. 2016;3:9.

7. Schulze-Bahr E, Eckardt L, Breithardt G, Seidl K, Wichter T, Wolpert C, et al. Sodium channel gene (SCN5A) mutations in 44 index patients with Brugada syndrome: different incidences in familial and sporadic disease. Hum Mutat. 2003;21(6):651-2.
8. Wang L, Han Z, Dai J, Cao K. Brugada Syndrome Caused by Sodium Channel Dysfunction Associated with a SCN1B Variant A197V. Arch Med Res. 2020;51(3):245-53.
9. Yan GX, Antzelevitch C. Cellular basis for the Brugada syndrome and other mechanisms of arrhythmogenesis associated with ST-segment elevation. Circulation. 1999;100(15):1660-6.
10. Wang Y, Liang P, Lan F, Wu H, Lisowski L, Gu M, et al. Genome editing of isogenic human induced pluripotent stem cells recapitulates long QT phenotype for drug testing. J Am Coll Cardiol. 2014;64(5):451-9.
11. Jans D, Callewaert G, Krylychkina O, Hoffman L, Gullo F, Prodanov D, et al. Action potential-based MEA platform for in vitro screening of drug-induced cardiotoxicity using human iPSCs and rat neonatal myocytes. J Pharmacol Toxicol Methods. 2017;87:48-52.
12. Matsa E, Rajamohan D, Dick E, Young L, Mellor I, Staniforth A, et al. Drug evaluation in cardiomyocytes derived from human induced pluripotent stem cells carrying a long QT syndrome type 2 mutation. Eur Heart J. 2011;32(8):952-62.
13. Selga E, Sendfeld F, Martinez-Moreno R, Medine CN, Tura-Ceide O, Wilmut SI, et al. Sodium channel current loss of function in induced pluripotent stem cell-derived cardiomyocytes from a Brugada syndrome patient. J Mol Cell Cardiol. 2018;114:10-9.
14. Liang P, Sallam K, Wu H, Li Y, Itzhaki I, Garg P, et al. Patient-Specific and Genome-Edited Induced Pluripotent Stem Cell-Derived Cardiomyocytes Elucidate Single-Cell Phenotype of Brugada Syndrome. J Am Coll Cardiol. 2016;68(19):2086-96.
15. Cui C, Geng L, Shi J, Zhu Y, Yang G, Wang Z, et al. Structural and electrophysiological dysfunctions due to increased endoplasmic reticulum stress in a long-term pacing model using human induced pluripotent stem cell-derived ventricular cardiomyocytes. Stem Cell Res Ther. 2017;8(1):109.
16. Cai C, Huang J, Lin Y, Miao W, Chen P, Chen X, et al. Particulate matter 2.5 induced arrhythmogenesis mediated by TRPC3 in human induced pluripotent stem cell-derived cardiomyocytes. Arch Toxicol. 2019;93(4):1009-20.
17. Antzelevitch C, Brugada P, Borggrefe M, Brugada J, Brugada R, Corrado D, et al. Brugada syndrome: report of the second consensus conference. Heart Rhythm. 2005;2(4):429-40.
18. Malhi N, Cheung CC, Deif B, Roberts JD, Gula LJ, Green MS, et al. Challenge and Impact of Quinidine Access in Sudden Death Syndromes: A National Experience. JACC Clin Electrophysiol. 2019;5(3):376-82.
19. Lieu DK, Fu JD, Chiamvimonvat N, Tung KC, McNerney GP, Huser T, et al. Mechanism-based facilitated maturation of human pluripotent stem cell-derived cardiomyocytes. Circ Arrhythm Electrophysiol. 2013;6(1):191-201.
20. Poon E, Yan B, Zhang S, Rushing S, Keung W, Ren L, et al. Transcriptome-guided functional analyses reveal novel biological properties and regulatory hierarchy of human embryonic stem cell-derived

ventricular cardiomyocytes crucial for maturation. PLoS One. 2013;8(10):e77784.

21. Kuppusamy KT, Jones DC, Sperber H, Madan A, Fischer KA, Rodriguez ML, et al. Let-7 family of microRNA is required for maturation and adult-like metabolism in stem cell-derived cardiomyocytes. Proc Natl Acad Sci U S A. 2015;112(21):E2785-94.
22. Wang J, Cui C, Nan H, Yu Y, Xiao Y, Poon E, et al. Graphene Sheet-Induced Global Maturation of Cardiomyocytes Derived from Human Induced Pluripotent Stem Cells. ACS Appl Mater Interfaces. 2017;9(31):25929-40.
23. Portero V, Casini S, Hoekstra M, Verkerk AO, Mengarelli I, Belardinelli L, et al. Anti-arrhythmic potential of the late sodium current inhibitor GS-458967 in murine Scn5a-1798insD+/- and human SCN5A-1795insD+/- iPSC-derived cardiomyocytes. Cardiovasc Res. 2017;113(7):829-38.
24. Dhar Malhotra J, Chen C, Rivolta I, Abriel H, Malhotra R, Mattei LN, et al. Characterization of sodium channel alpha- and beta-subunits in rat and mouse cardiac myocytes. Circulation. 2001;103(9):1303-10.
25. Kosmidis G, Veerman CC, Casini S, Verkerk AO, van de Pas S, Bellin M, et al. Readthrough-Promoting Drugs Gentamicin and PTC124 Fail to Rescue Nav1.5 Function of Human-Induced Pluripotent Stem Cell-Derived Cardiomyocytes Carrying Nonsense Mutations in the Sodium Channel Gene SCN5A. Circ Arrhythm Electrophysiol. 2016;9(11).
26. Davis RP, Casini S, van den Berg CW, Hoekstra M, Remme CA, Dambrot C, et al. Cardiomyocytes derived from pluripotent stem cells recapitulate electrophysiological characteristics of an overlap syndrome of cardiac sodium channel disease. Circulation. 2012;125(25):3079-91.
27. Nakaya H. SCN5A mutations associated with overlap phenotype of long QT syndrome type 3 and Brugada syndrome. Circ J. 2014;78(5):1061-2.
28. Broyles CN, Robinson P, Daniels MJ. Fluorescent, Bioluminescent, and Optogenetic Approaches to Study Excitable Physiology in the Single Cardiomyocyte. Cells. 2018;7(6).
29. Kopljar I, Lu HR, Van Ammel K, Otava M, Tekle F, Teisman A, et al. Development of a Human iPSC Cardiomyocyte-Based Scoring System for Cardiac Hazard Identification in Early Drug Safety De-risking. Stem Cell Reports. 2018;11(6):1365-77.
30. Sieira J, Dendramis G, Brugada P. Pathogenesis and management of Brugada syndrome. Nat Rev Cardiol. 2016;13(12):744-56.
31. Belhassen B, Glick A, Viskin S. Efficacy of quinidine in high-risk patients with Brugada syndrome. Circulation. 2004;110(13):1731-7.
32. Vicente J, Johannesen L, Mason JW, Crumb WJ, Pueyo E, Stockbridge N, et al. Comprehensive T wave morphology assessment in a randomized clinical study of dofetilide, quinidine, ranolazine, and verapamil. J Am Heart Assoc. 2015;4(4).
33. Hai JJ, Wong CK, Chan PH, Tse HF, Yung TC, Siu CW. Quinidine for Brugada syndrome: Panacea or poison? HeartRhythm Case Rep. 2016;2(6):486-90.
34. Nishida A, Takizawa T, Matsumoto A, Miki T, Seino S, Nakaya H. Inhibition of ATP-sensitive K+ channels and L-type Ca2+ channels by amiodarone elicits contradictory effect on insulin secretion in

MIN6 cells. J Pharmacol Sci. 2011;116(1):73-80.

35. Page G, Ratchada P, Miron Y, Steiner G, Ghetti A, Miller PE, et al. Human ex-vivo action potential model for pro-arrhythmia risk assessment. J Pharmacol Toxicol Methods. 2016;81:183-95.
36. Szel T, Antzelevitch C. Abnormal repolarization as the basis for late potentials and fractionated electrograms recorded from epicardium in experimental models of Brugada syndrome. J Am Coll Cardiol. 2014;63(19):2037-45.
37. Martin CA, Guzadhur L, Grace AA, Lei M, Huang CL. Mapping of reentrant spontaneous polymorphic ventricular tachycardia in a Scn5a+/- mouse model. Am J Physiol Heart Circ Physiol. 2011;300(5):H1853-62.
38. Nishida K, Fujiki A, Mizumaki K, Sakabe M, Sugao M, Tsuneda T, et al. Canine model of Brugada syndrome using regional epicardial cooling of the right ventricular outflow tract. J Cardiovasc Electrophysiol. 2004;15(8):936-41.

Figures

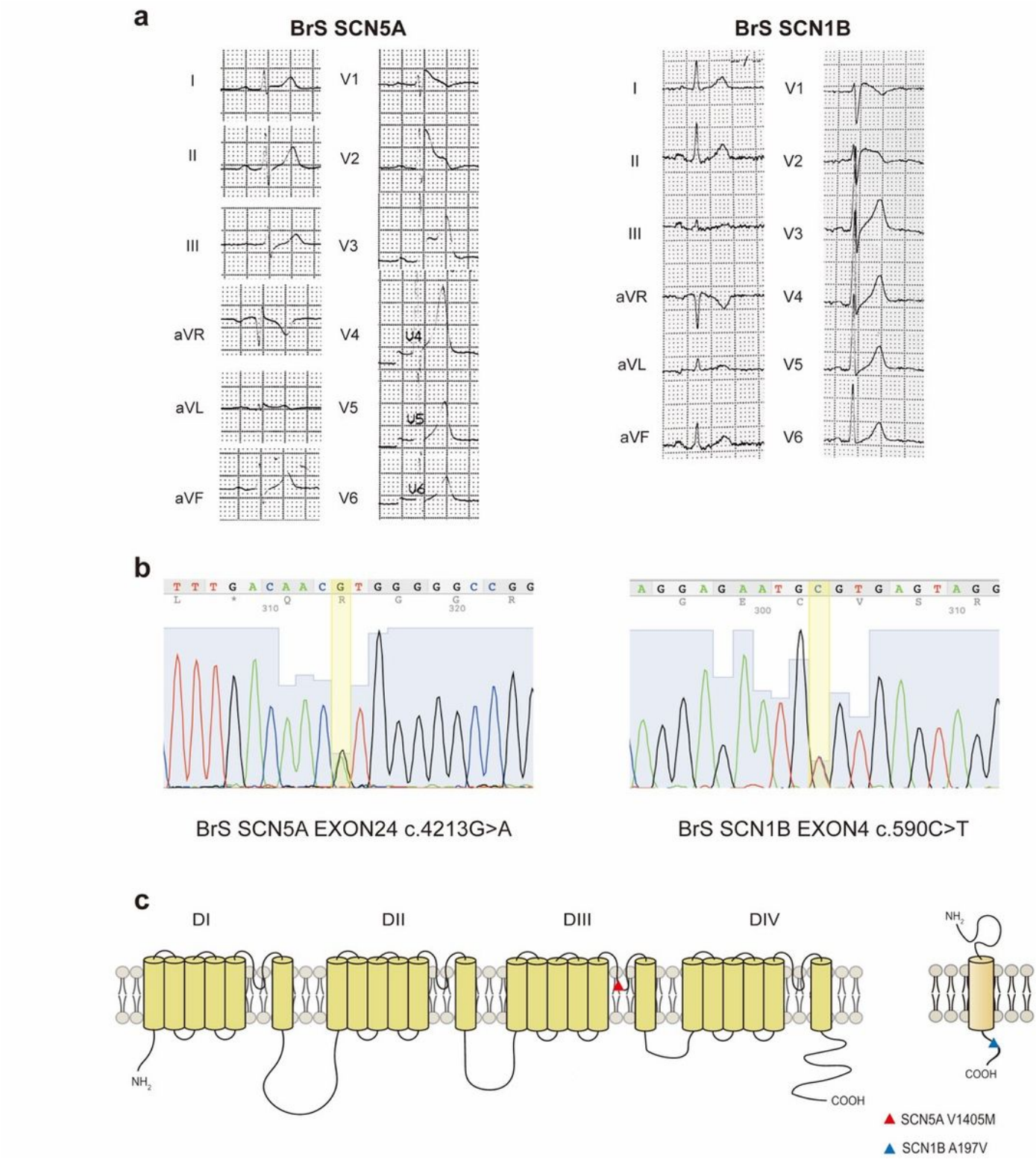

Figure 1

Clinical and genetical profile of the two BrS patients. a. Electrocardiograms of both patients show the typical ST segment elevation, a typical pattern of Brugada syndrome. b. Genotyping of hiPSC SCN5A and hiPSC SCN1B lines focusing on the loci around each mutation confirmed by DNA sequencing. c. The corresponding positions of V1405M mutation on the protein structure of voltage-gated sodium-channel α subunit gene (right panel), and A197V mutation on the ß1 subunit gene.

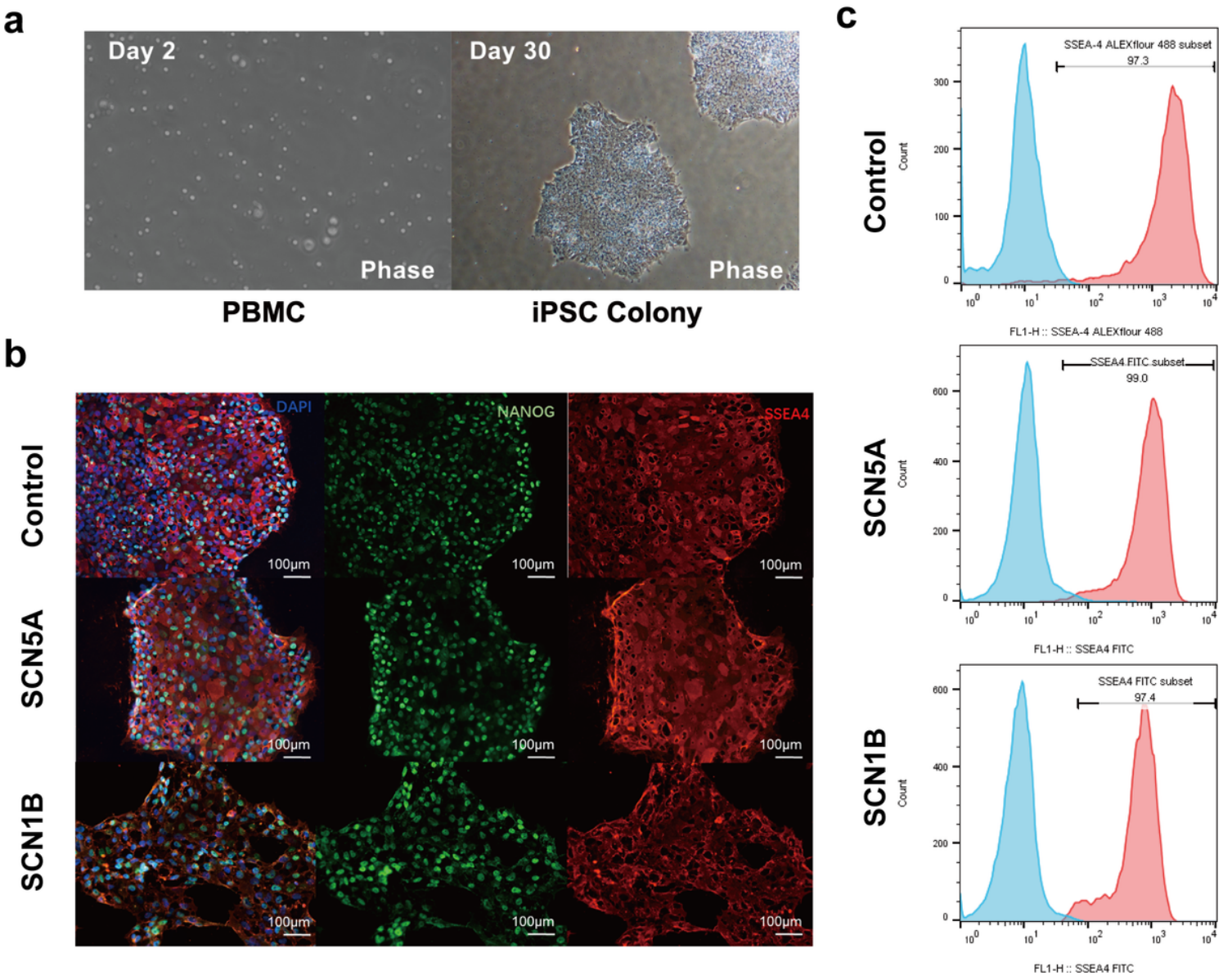

Figure 2

Basic characterization of hiPSC lines. a. Representative bright field images of PBMC and iPSC colony derived from BrS1 patient in feeder free culture condition. b. Images of iPS cells stained with pluripotency markers NANOG (green), SSEA4 (red) for healthy control, hiPSC-SCN5A and hiPSC-SCN1B lines. Nuclei were stained with DAPI (blue). Scale bars represent 100 µm. c. Flow cytometry analysis of pluripotency markers (SSEA4) in generated iPSC lines.

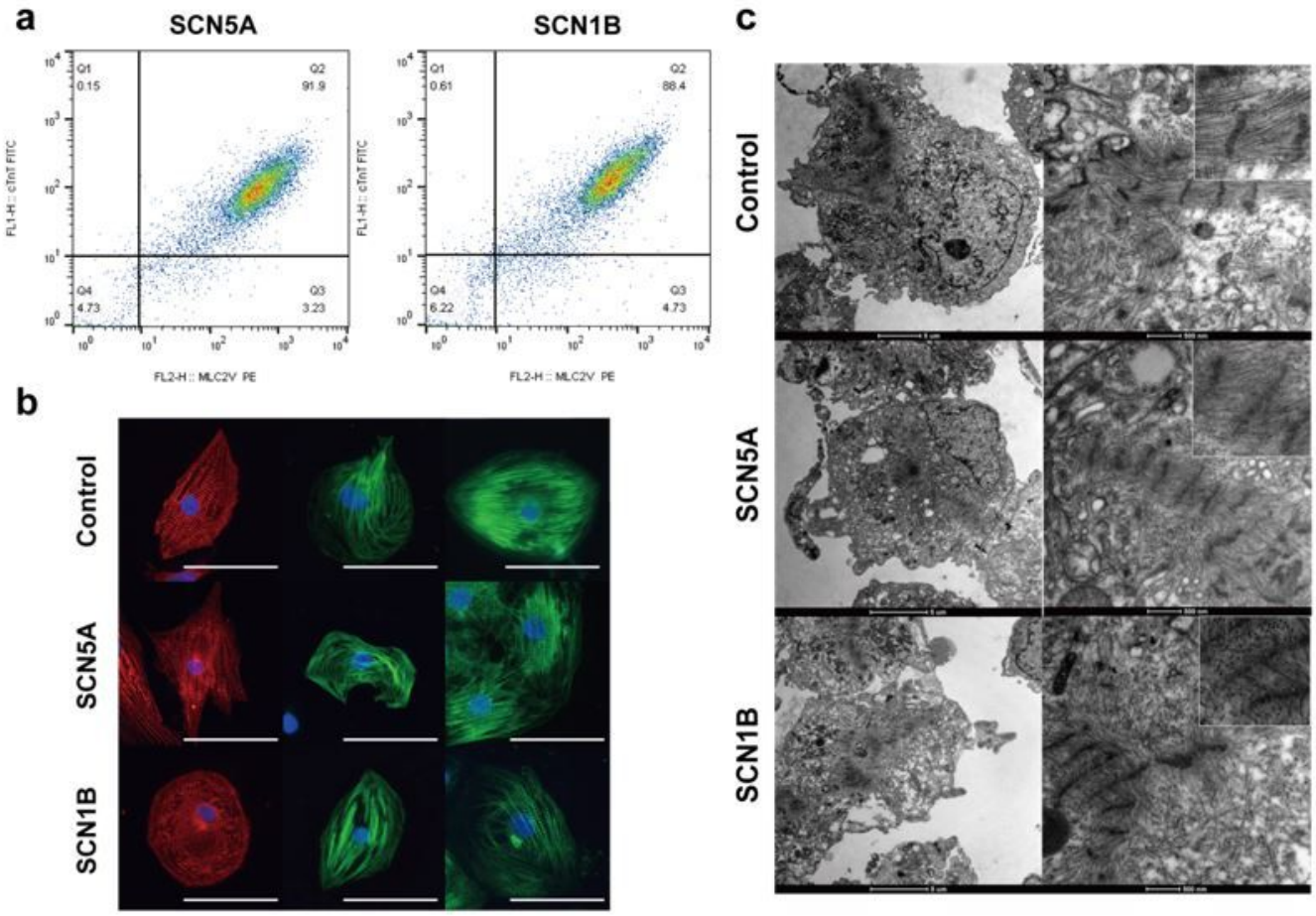

Figure 3

Differentiation of hiPSC lines into the cardiac lineage. a. Representative flow cytometry confirming the high percentage of ventricular myocytes in differentiated cells. b. Immunostaining of sarcomeric α-actinin, cTnI and MLC2v at day 30 post differentiation. Scale bars represent 50um. c. TEM images of myofibrillar organization in control and BrS iPSC-CMs.

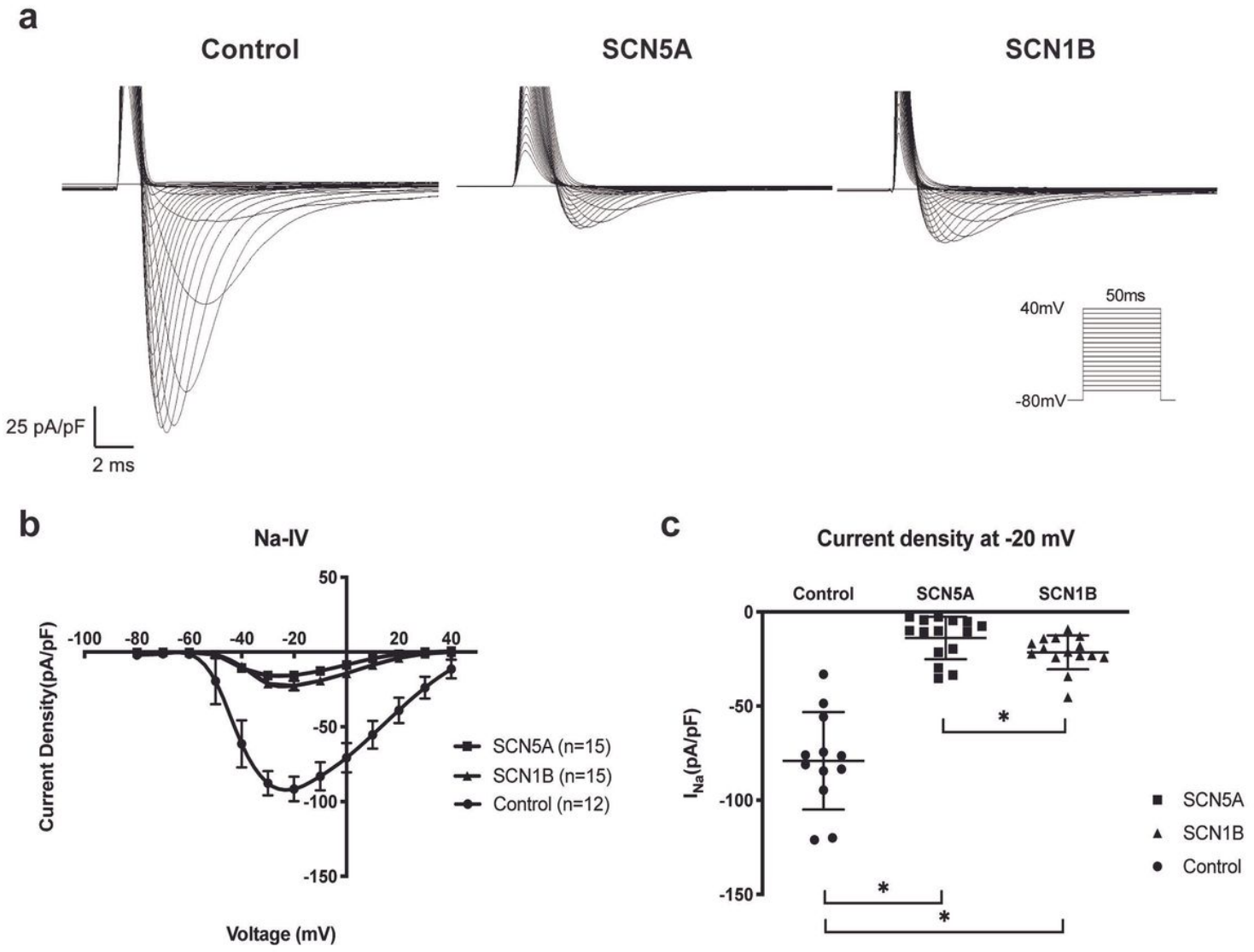

Figure 4

iPS-CMs carrying SCN5A or SCN1B mutation showed impaired INa properties. a. Typical INa curve measured by the voltage clamp protocol. Traces for pulses from −80 mV to −40 mV are shown. b. Current–voltage relationships of INa from control, hiPSC-SCN5A and hiPSC-SCN1B normalized to the cell capacitance. c. Comparison of INa density at -20 mV between control and the BrS lines. *P < 0.05 according to a one-way ANOVA test.

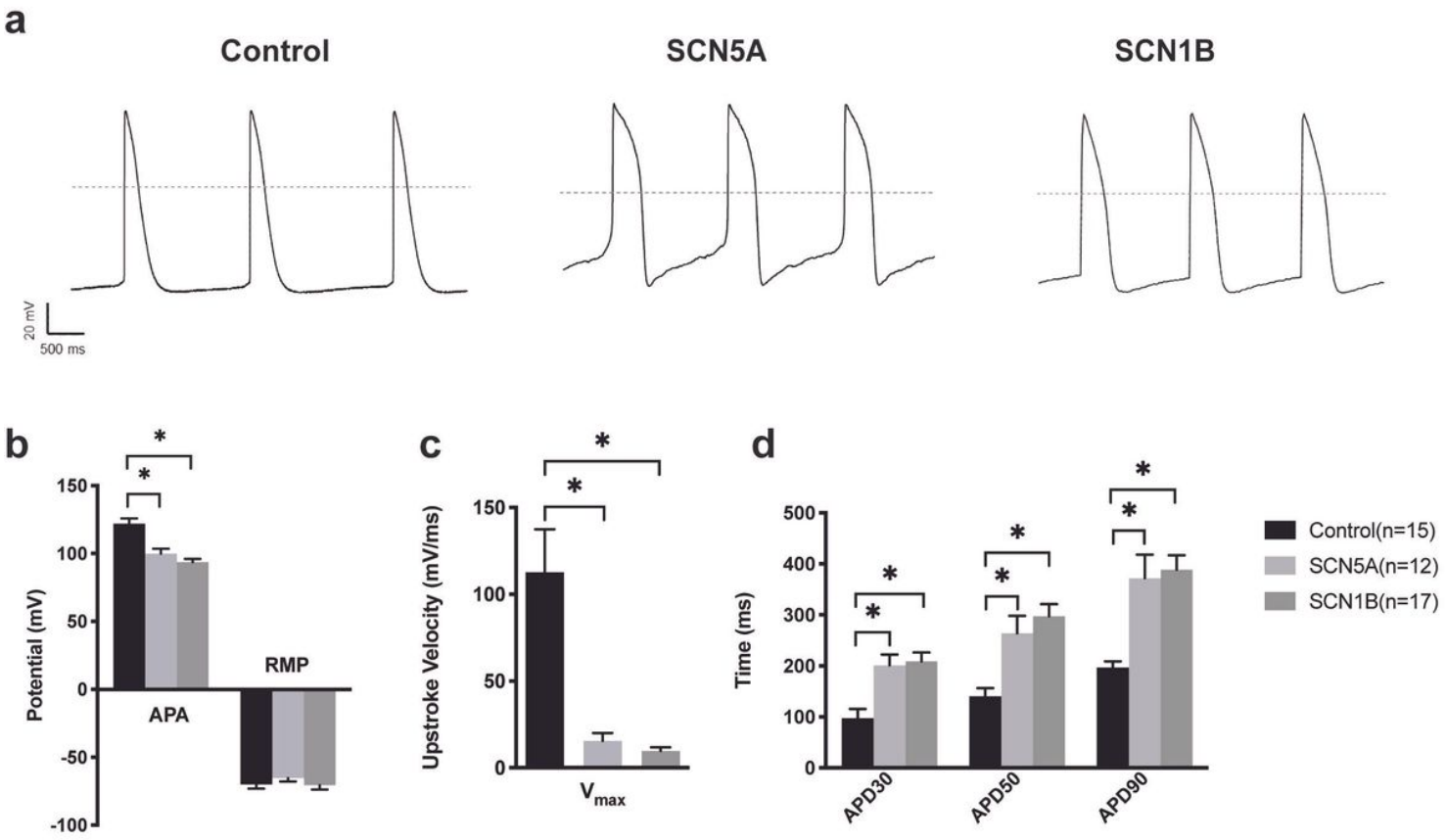

Figure 5

Prolonged action potential durations and decreased Vmax in both BrS iPSC-CMs. a. Representative spontaneous AP traces in control and BrS myocytes using current-clamp recording. Dotted line indicates 0 mV. b,c,d: Mean values for APA, RMP, Vmax and APD at 30%, 50% and 90% repolarization (APD30, APD50, APD90) in control and SCN5A, SCN1B cell lines. n=11 for control * P□0.05 according to a one-way ANOVA test.

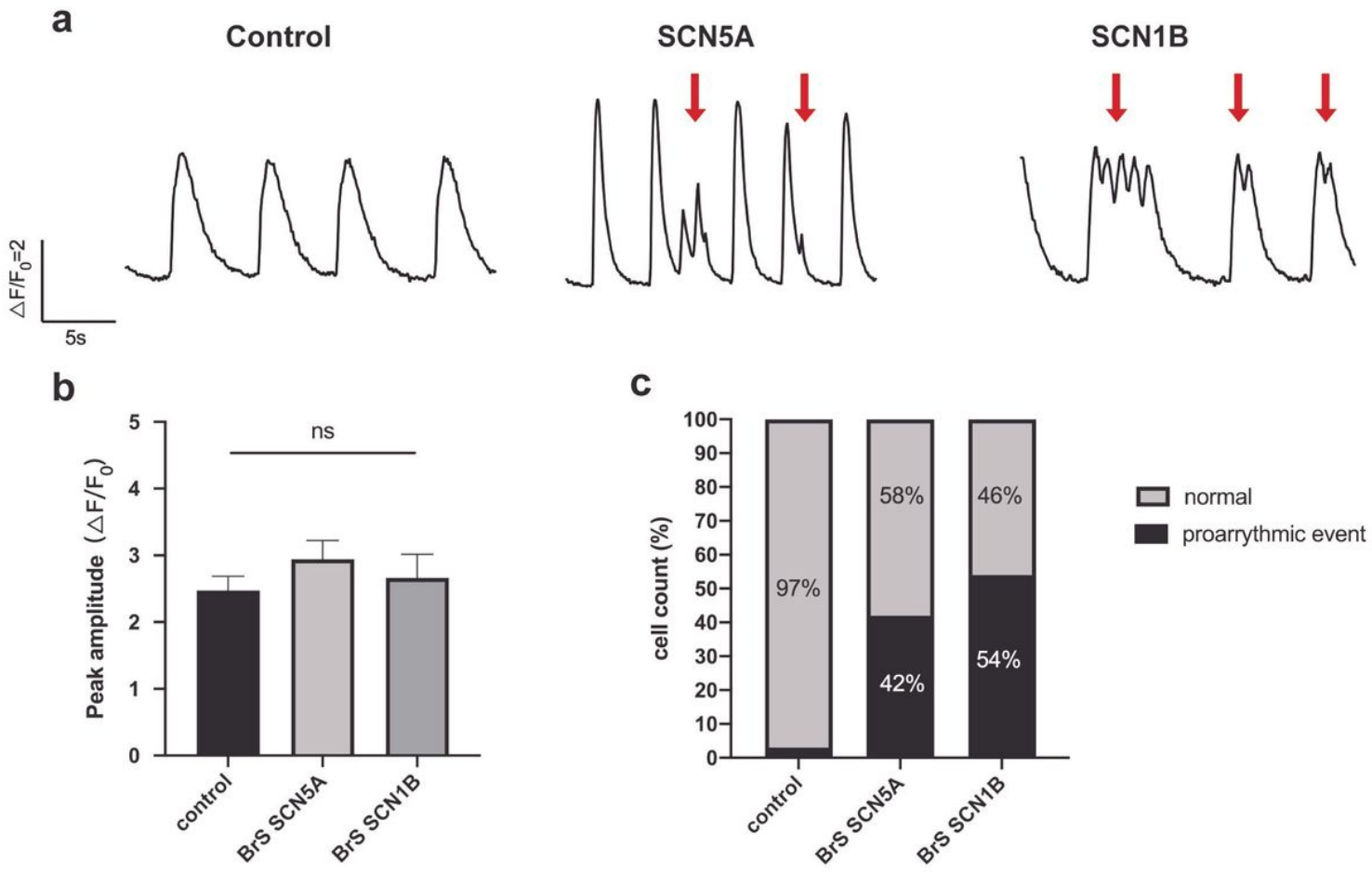

Figure 6

both BrS iPSC-CMs exhibited abnormal Ca2+ handling. a. Representative spontaneous Ca2+ transients in control and BrS iPSC-CMs, red arrow indicates early afterdepolarization-like or delayed afterdepolarization-like activities. b. Peak amplitude of spontaneous Ca2+ transients in control and BrS iPSC-CMs. (n=30 for each line) c. Percentages of cells showing proarrhythmic (triggered) events in each line.

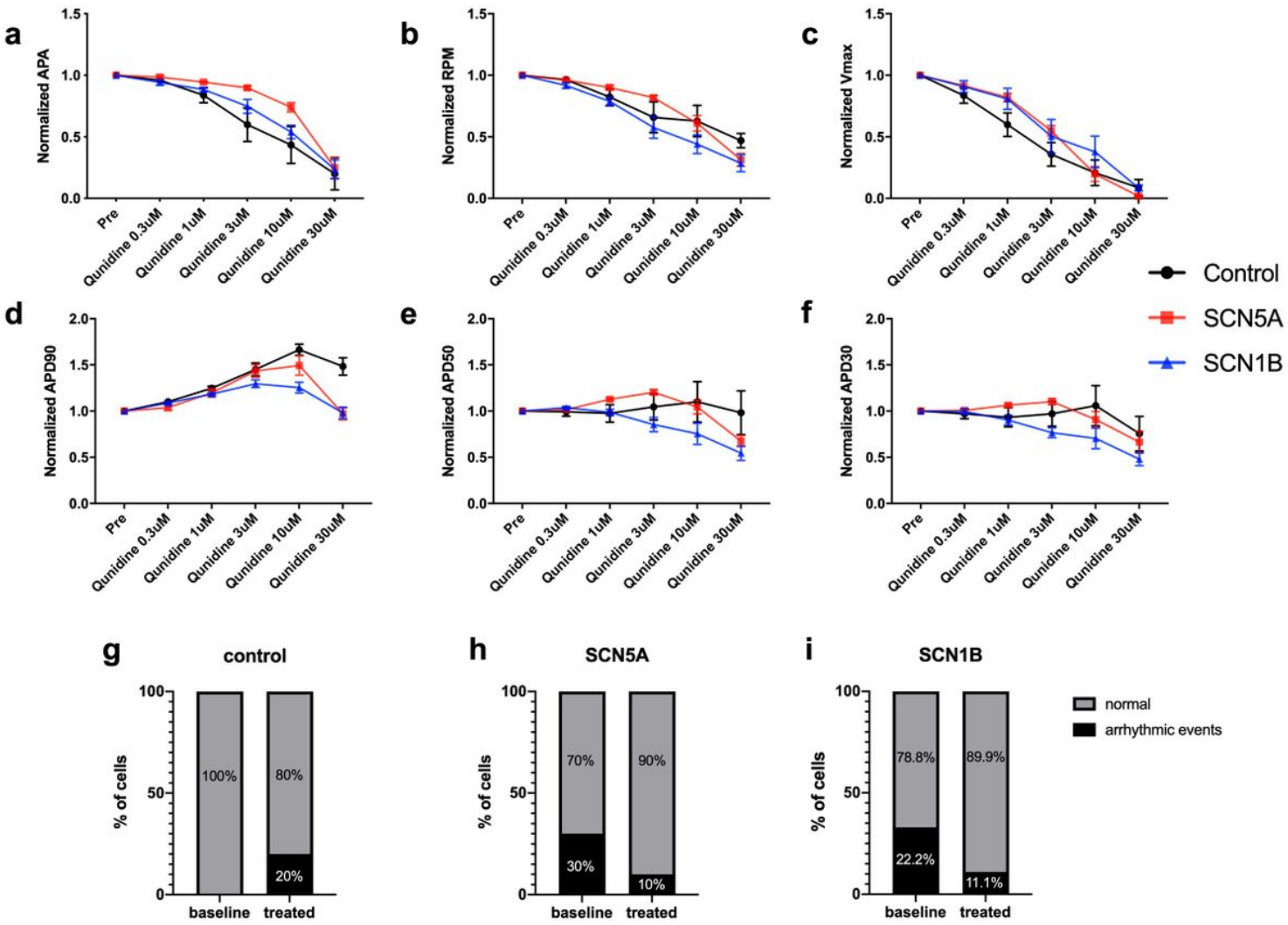

Figure 7

iPSC-CMs in response to escalating concentrations of quinidine. Quinidine-treated CMs exhibited the reduction of APA(a.), RPM(b.), Vmax(c.), and the prolongation of APD90(d.) in all cell lines after standardization. g~i.: Percentage of cardiomyocytes displaying arrhythmic events at baseline and after treating with quinidine. (Control: n=10 cells; BrS-SCN5A: n=10 cells; BrS-SCN1B: n=9 cells).

Supplementary Files

This is a list of supplementary files associated with this preprint. Click to download.

- TableS2.docx
- TableS1.docx
- FigureS3.docx
- FigureS2.docx
- FigureS1.docx

- Supplementaryfile.docx